Article:

Yuan, R, Yu, H-S orcid.org/0000-0003-3330-1531, Zhang, J-R et al. (1 more author) (2019) Noncoaxial Theory of Plasticity Incorporating Initial Soil Anisotropy. International Journal of Geomechanics, 19 (12). 06019017. ISSN 1532-3641

https://doi.org/10.1061/(asce)gm.1943-5622.0001513

Non-coaxial theory of plasticity incorporating initial anisotropy

Ran Yuan[1], Hai-Sui Yu[2], Jia-Rong Zhang[3], Yong Fang[4]*

[1] Assistant Professor, Key Laboratory of High-speed Railway Engineering of Ministry of Education, Southwest Jiaotong University, 610031, Chengdu, China. Email: yuanran@swjtu.edu.cn.

[2] Professor, School of Civil Engineering, University of Leeds, Leeds LS2 9JT, UK. Email: h.yu@leeds.ac.uk.

[3] PhD candidate, Key Laboratory of High-speed Railway Engineering of Ministry of Education, Southwest Jiaotong University, 610031, Chengdu, China. Email: JRDoggy@my.swjtu.edu.cn.

[4] Professor, Key Laboratory of Transportation Tunnel Engineering of Ministry of Education, Southwest Jiaotong University, 610031, Chengdu, China. E-mail: fy980220@swjtu.cn.

*Corresponding Author

ABSTRACT

In this paper, a non-coaxial, plane strain soil model is developed in the framework of initial soil strength anisotropy that is described by taking the internal friction angle to be a function of principal stress orientations. The conventional Mohr-Coulomb (M-C) yield criterion is generalized to give an anisotropic yield criterion, with the curve in the deviatoric stress space forming an ellipse. Both rotational and eccentric ellipses are discussed. The formulation of non-coaxial constitutive equations is described by a general form in terms of the plastic strain rate. In this form, the plastic strain rate is divided into two parts: the conventional component that is derived from the classical plastic potential theory, and the non-coaxial component that is assumed to be tangential to the yield surface. The newly proposed model is validated by the analytical calculations and DEM simulation results in simple shear tests. Conclusions can be drawn that this model is generally capable of capturing the DEM observations of simple shear testing.

INTRODUCTION

The foundation of classical plasticity theory was laid in the 1950s and 1960s. One of the key concepts of the theory assumed that the principal stress and plastic strain rate directions are coaxial, as reviewed by Yu (2007). Normally geotechnical applications are performed in the content of soil coaxiality (e.g., Wu et al 2019; He et al 2019). Recent experimental research (e.g., Roscoe et al. 1967; Roscoe 1970; Tong et al 2010; Yang 2013) and micro-mechanical evidence (e.g., Drescher and De Josselin de Jong 1972; Zhang 2003; Ai et al 2014) have found that during rotations of the principal stresses, the principal axes of strains rotate as well; however, generally they do not coincide with each other. Non-coincidence of orientations of the principal stress and plastic strain rate was thereafter classified in the plasticity theory as non-coaxiality.

A number of constitutive models have been proposed to incorporate non-coaxial plasticity through phenomenological or multi-scale approaches. In the past, non-coaxial models were developed in the framework of soil isotropy, e.g., non-coaxial models based on the yield vertex theory (Yang and Yu, 2006a) and the double shearing theory (Yu and Yuan, 2006), the hypoplastic constitutive law enhanced by mirco-polar terms to account for the non-coaxiality (Tejchman and Wu, 2009), modified multi-laminate models taking into account the rotation of the principal stress axes (Pande and Sharma, 1983; Neher, et al., 2002) and others (Borja, et al., 2003; Qian, et al., 2008; Huang, et al., 2010). Many researchers suggested that the intrinsic fabric of soils is anisotropic, where soil particles tend to be aligned in some preferred directions during deposition (e.g., Arthur, et al., 1977; Cai, et al., 2012; Yang, 2013). Recent studies have demonstrated the necessity of incorporating both anisotropy and non-coaxiality to simulate soil behaviour subjected to severe stress rotations (Li and Dafalias, 2004; Tsutsumi and Hashiguchi, 2005; Sadrnejad and Shakeri, 2017).

Although many non-coaxial models in the literature have been developed for granular materials, they have not been widely applied to investigate boundary value problems. Indeed, aforementioned non-coaxial models developed through a phenomenological approach often introduce too many parameters without physical meanings and are difficult for calibration; while in the models developed through a multi-scale approach (e.g., fabric tensor-based constitutive models), the effects of fabric anisotropy and non-coaxiality are described by quantities light on clear physical meanings.

A particular literature can be referred to Yang and Yu (2006a; 2006b; 2010), who performed a series of numerical evolutions of a couple of pre-failure, non-coaxial models. The simple formulations of their models allowed them to be used in analyzing geotechnical problems (Yang and Yu, 2006c). Nevertheless, their models are restricted to initial soil isotropy characterized by the conventional Mohr-Coulomb (M-C) criterion.

In this paper, a plane strain, perfect plasticity non-coaxial model is developed, in which the conventional isotropic M-C yield criterion has been generalized to incorporate the effects of initial soil strength anisotropy. Two more material parameters are added to those of the conventional isotropic M–C yield criterion to form an anisotropic yield criterion. Both parameters demonstrate clear physical meanings and can be easily calibrated. The validation of this newly developed model is performed by comparing the numerical results of simple shear problems with analytical results and Discrete Element Method (DEM)-based virtual experimental observations.

CONSTITUTIVE EQUATIONS OF THE MODEL

A non-coaxial, plane strain model is developed in the content of initial soil strength anisotropy. The elastic part follows Hooke's model. All stresses are assumed to be effective stresses and the signs of the stress (rate) are chosen to be positive for tension.

The anisotropic yield criterion

The shape in the stress space of $(\frac{\sigma_x-\sigma_y}{2}, \sigma_{xy})$ is a circle for the conventional isotropic M-C yield criterion, of which the radius only depends on the mean pressure p. However, in a significant paper, Booker and Davis (1972) developed a general anisotropic yield criterion, where the curve in the stress space of $(\frac{\sigma_x-\sigma_y}{2}, \sigma_{xy})$ was assumed to be a function of p and Θ_p. Θ_p refers to the angle between the major principal compressive stress direction and the y-axis. Θ_p is updated during the process of shearing and can be defined by:

$$\cos 2\Theta_p = \frac{\sigma_x-\sigma_y}{[(\sigma_x-\sigma_y)^2+4\sigma_{xy}^2]^{1/2}} \text{ and } \sin 2\Theta_p = \frac{2\sigma_{xy}}{[(\sigma_x-\sigma_y)^2+4\sigma_{xy}^2]^{1/2}} \qquad (1)$$

Similarly, the direction of principal plastic strain rate $\Theta_{\dot{\varepsilon}^p}$ can be defined by:

$$\tan 2\Theta_{\dot{\varepsilon}^{\mathrm{p}}} = \frac{2\dot{\varepsilon}_{\mathrm{xy}}^{\mathrm{p}}}{\dot{\varepsilon}_{\mathrm{x}}^{\mathrm{p}} - \dot{\varepsilon}_{\mathrm{y}}^{\mathrm{p}}} \tag{2}$$

Stresses are denoted by (σ_x, σ_y, σ_{xy}), and it is assumed to be impossible to attain states of stress lying outside the yield surface. As many laboratory experimental results (e.g., Yang 2013) gave that the internal friction angle is changing with the change of principal stress directions, the anisotropic yield criterion can be written in the following general form, when plane strain conditions are assumed (with tension positive):

$$\mathrm{f}(\sigma_{\mathrm{x}}, \sigma_{\mathrm{y}}, \sigma_{\mathrm{xy}}) = \mathrm{R} + \mathrm{F}(\mathrm{p}, \Theta_{\mathrm{p}}) = 0 \tag{3}$$

Where

$$\mathrm{F}(\mathrm{p}, \Theta_{\mathrm{p}}) = (\mathrm{p} - \mathrm{c}\cot\phi_{\mathrm{max}}) \cdot \sin\phi(\Theta_{\mathrm{p}}) \tag{4}$$

and $R = \frac{1}{2}[(\sigma_x - \sigma_y)^2 + 4\sigma_{xy}^2]^{1/2}$, p=$\frac{1}{2}(\sigma_x+\sigma_y)$, $\tan(2\Theta_p)=2\sigma_{xy}/(\sigma_x-\sigma_y)$, c denotes the cohesion.

As shown in Fig. 1b, the anisotropic yield curve in the deviatoric stress space is assumed as a rotational ellipse with a rotation angle of 2 β. With respect to the rotational ellipse, parameters ϕ_{max} and ϕ_{min} represent the maximum and minimum peak internal friction angles, respectively along all possible major principal stress directions. The semi-major and semi-minor ellipse lengths are denoted as L_{max} and L_{min} (Fig.1b). To define the anisotropic yield criterion, two anisotropic parameters n and β are added to those material properties of the conventional isotropic M-C yield criterion:

- n= L_{min}/ L_{max} = $\sin\phi_{min}/\sin\phi_{max}$, and $0<n\leq1$. This parameter is to quantify the degree of strength anisotropy. The smaller the value of n is, the larger the degree of initial strength anisotropy is. In particular, the conventional isotropic M-C yield criterion is recovered when n=1.0.
- β is denoted as the angle when the major compressive principal stress, corresponding to the case of the maximum peak internal friction angle, is inclined to the vertical direction in a Cartesian coordinate; and β ranges from 0 to $\frac{\pi}{4}$ (Yang, 2013).

Both n and β depend on the intrinsic micro-structure characteristics of soils and history of constitution (e.g., sedimentation; tectogenesis) of the soils. The parameter β is not updated with the changing of loading paths.

In this situation, the expression of $\sin\phi(\Theta_p)$ in Equation 4 can be derived by geometric considerations as follows:

$$\sin\phi(\Theta_p) = \frac{n\sin\phi_{max}}{\sqrt{n^2\cos^2(2\Theta_p - 2\beta) + \sin^2(2\Theta_p - 2\beta)}} \tag{5}$$

It is suggested by the Hollow Cylinder Apparatus (HCA) experimental results that the peak internal friction angle reduces with increasing α and it has a slight rebound at α=90°, when the intermediated principal stress parameter ($b=(\sigma_2-\sigma_3)/(\sigma_1-\sigma_2)$) is given (e.g., Yang 2013). Here α represents the direction of the major principal stress relative to the vertical:

$$\alpha = \frac{1}{2}tan^{-1}(2\tau_{\theta z})/(\sigma_z - \sigma_\theta) \tag{6}$$

The maximum magnitude of the peak internal friction angle is obtained when the major principal stress direction lies between $2\beta=0$-$\pi/2$, so we constrain the value of β to drop between 0-$\pi/4$. Moreover, it should be noted that the formulation of the rotational ellipse to describe initial strength anisotropy is just one particular case of the anisotropic yield criterion. Other types of ellipses are possible. An eccentric ellipse anisotropic yield criterion can be introduced to complement the proposed type. The formulation of the yield surface is similar to the proposed case. The only difference in the formulation of the yield criterion when compared with the rotational ellipse will be the definition of $\sin\phi(\Theta_p)$:

$$\sin\phi(\Theta_p) = \frac{n^2 S_b \cos 2\Theta_p + \sqrt{n^4 S_a{}^2 \cos^2(2\Theta_p) + 4n^2\sin^2(2\Theta_p)\sin\phi_{max}\sin\phi_p}}{2n^2\cos^2(2\Theta_p) + 2\sin^2(2\Theta_p)} \tag{7}$$

and

$$S_a = \frac{1}{2}(\sin\phi_{max} + \sin\phi_p) \tag{8}$$

$$S_b = \frac{1}{2}(\sin\phi_{max} - \sin\phi_p) \tag{9}$$

where ϕ_p denotes the internal friction angle obtained when $\Theta_p=\pi/2$, ϕ_{max} denotes the maximum peak internal friction angle and n represents the ratio of the minor axis divided by the major axis of the ellipse ($0<n\leq1$).

Details of the validation can be referred to Yuan et al (2018).

Non-coaxial plastic flow rule

Following Yu and Yuan (2006), the total plastic strain rate is composed by: 1) the conventional part that is derived from the classical plastic potential theory; 2) the non-coaxial part caused by stress rates that is tangential to the yield curve. The plastic strain rate $\dot{\boldsymbol{\varepsilon}}^p$ is generally shown as (Fig.2):

$$\dot{\boldsymbol{\varepsilon}}^p = \dot{\lambda}\,\frac{\partial \mathrm{g}}{\partial \boldsymbol{\sigma}} + k \cdot \dot{\boldsymbol{T}} \quad \text{if } f = 0 \quad \text{and } \dot{f} = 0 \tag{10}$$

Where $\dot{\lambda}$ is a positive scalar and g denotes the plastic potential; k is a non-coaxial coefficient; $\dot{\boldsymbol{T}}$ is the material derivative dependent on the tangential stress state, which is a function of the direction of principal stresses and the internal friction angle. Details of the tangential and conventional component of the plastic strain rate can be found in the Appendix.

With respect to non-associativity in the conventional plastic flow rule (g ≠ f), the plastic potential (g) takes the variation of dilation angle into account. The dilation angle is taken to be a function of principal stress directions, and varies between zero and the value of the corresponding internal friction angle. The plastic potential is displayed as:

$$\mathrm{g} = \sqrt{\frac{1}{4}(\sigma_y - \sigma_x)^2 + \sigma_{xy}^2} + \frac{1}{2}(\sigma_x + \sigma_y)\sin\psi(\Theta_p) = \text{constant}, \tag{11}$$

and

$$\sin\psi(\Theta_p) = \frac{\mathrm{n}\cdot\sin\psi_{max}}{\sqrt{\mathrm{n}^2\cdot\cos^2(2\Theta_p - 2\beta) + \sin^2(2\Theta_p - 2\beta)}} \tag{12}$$

where ψ_{max} denotes the maximum dilation angle.

Summary of parameters

Three new parameters, i.e. β, n and k, are introduced by the new non-coaxial soil model. Various values of strength with direction (at least three) can be obtained from plane strain monotonic loading tests, e.g., biaxial testing or HCA testing. These values of strength with direction can be substituted in the yield function to calculate β, n and ϕ_{max}. If experimental data is sufficient, two anisotropic parameters β and n can be obtained using the nonlinear regression analysis, to guarantee the accuracy and validate the anisotropic yield criterion. The non-coaxial parameter k can be obtained by analyzing the stress-strain results from laboratory testing subjected to principal stress rotations, e.g., simple shear testing or HCA testing. As analyzed by Yu (2007), k can be determined based on the double shearing theory (Spencer, 1964; Harris, 1993) and the yield-vertex flow rule proposed by Rudnicki and Rice (1975).

VALIDATION IN SIMPLE SHEAR TESTS

As the soil sample under simple shear loading is subject to a severe principal stress rotation, the numerical validation of the newly proposed non-coaxial model can be conducted using simple shear problems. For simplicity, a single isoparametric, eight-noded, plane strain reduced integration element CPE8R is used. All of the sides remain linear, and the top and bottom are kept parallel to their original directions throughout loading. The bottom nodes are fixed and neither vertical nor horizontal movements are allowed under this assumption. A prescribed shear strain γ_{xy} is employed and the x-direction is constrained to have zero direct strain (ε_x=0). Hence, the sample is subjected to a rotation of the principal stress caused by the change in the induced shear stress τ_{xy}. It should be noted here that σ_x is equal to σ_z throughout the shearing due to the adoption of the plane strain condition in the z-direction and full constraining of the movement in the x-direction. Loading and boundary conditions are both based on ideal assumptions since the objective of this paper is to numerically validate the proposed non-coaxial soil model.

The explicit form of an incremental stress-strain relationship of the newly proposed non-coaxial model is implemented as a user subroutine in a commercial finite element code ABAQUS. By introducing one parameter a ($a \leq c\cot\phi$) (Abbo, 1997), the yield criterion is modified with a hyperbolic approximation to eliminate singularity. A close straight line that defines the anisotropic yield surface can be obtained by using an asymptotic hyperbola. The modified yield criterion can be shown as:

$$f = \sqrt{(\frac{\sigma_x - \sigma_y}{2})^2 + \sigma_{xy}^2 + a^2\sin^2\phi(\Theta_p)} + (p - c\cot\phi_{max})\sin\phi(\Theta_p) = 0 \qquad (13)$$

Where the negative branch of the hyperbola has been chosen.

The explicit sub-stepping integration algorithm with automatic error controls is applied for the numerical implementation. If the stresses diverge from the yield condition at the end of each subincrement in the integration process, correcting for this violation from the yield surface is required. The correction is carried out following the method suggested by Abbo (1997). However, as the tangential effect is considered in this paper, the isotropic stiffness matrix $\mathbf{D_e}$ in Abbo's suggestion should be replaced by the modified elastic stiffness matrix ($\overline{\boldsymbol{D}^{e}}$) in Equation 39 (Appendix).

Yu and Yuan (2006) reviewed the studies carried out by Anand (1983) and Savage and Lockner (1997), and they noticed that it is necessary to relax the original kinematic hypothesis that slip lines coincide with stress characteristics to allow the double shearing concept to be used more successfully in the range of pre-failure deformation. Following the analysis of Harris (1993), they assumed that the non-coaxial soil coefficient in their non-coaxial model would take a positive value if the stress and velocity characteristic directions are different. In this paper, the value of the non-coaxial soil coefficient k is taken as a positive constant. A cohesionless material is assumed in this section. In order to avoid the singularity problem for numerical modelling in ABAQUS, the value of cohesion is set as 0.001 kPa.

Validation with analytical results (n=1.0)

Material constants are set as the same as those used by Hansen (1961) to validate the accuracy, and the finite element formulation and solution procedures. When associativity is applied, the dilation angle $\psi(\Theta_p)$ equals to the friction angle $\phi(\Theta_p)$. Yu and Yuan (2006) argued that the degree of non-associativity has negligible effects on the numerical simulations. Hence, $\psi(\Theta_p)$ is set to 0° for simplicity when non-associativity is applied. Typical mode parameters are shown in Table 1.

The model is reduced to its isotropic counterpart when the anisotropic parameter n =1.0. Davis (1968) proposed that for a purely frictional soil on the slip line, the M-C failure criterion can be described by the following stress ratio:

$$\left(\frac{\sigma_{xy}}{\sigma_y}\right)_{\text{ultimate}} = \frac{\sin\phi\cos\psi}{1-\sin\phi\sin\psi} \tag{14}$$

where ϕ is the friction angle and ψ refers to the dilation angle.

The ultimate values of the shear stress ratio are $(\sigma_{xy}/\sigma_y)_{ultimate}$=0.577 (Fig. 3(a)) and $(\sigma_{xy}/\sigma_y)_{ultimate}$=0.499 (Fig. 3(b)) by using associativity and non-associativity, respectively. These values are consistent with analytical results calculated from Equation 14. The lateral stress ratio K_0 has negligible effects on the ultimate shear stress ratio. If K_0 = 2.0, In addition, the peak of shear stress ratio is obtained as $(\sigma_{xy}/\sigma_y)_{peak}$=0.577 (Fig. 3(b)), which agrees well with analytical results calculated by Hansen (1961) with $(\sigma_{xy}/\sigma_y)_{peak}$= tan$\phi$ ($\phi = 30^o$). A strain-softening can be observed in Fig. 3(b), when K_0>1.0 in combination with non-associativity are used. The softening of the shear stress ratio occurs because the initial σ_x (i.e., $2\sigma_y$) is larger than its ultimate value (σ_y). Given certain shear strength in the general stress space, a larger σ_x (σ_z) can bear a larger shear stress during the early stage of shearing. Both the coaxial and non-coaxial predicted stress-strain curves tend to reach the same value at the ultimate stage during the process of shearing.

As shown in Fig. 4, with coaxial plasticity, the principal plastic strain rate direction is always identical with the principal stress direction. The ultimate principal stress and principal plastic strain rate orientations to the x−axis approach 60^o when associativity is used, and 45^o when non-associativity is used. They are in agreement with the theoretical study of Davis (1968), who pointed out that, at the ultimate failure, any horizontal plane (i.e. a velocity characteristic) is always inclined at 45^o+ψ/2 with respect to the principal axis of the stress. The orientation is between 0^o and 45^o+ψ/2 for K_0=0.5; whereas, the orientation is between 45^o+ψ/2 and 90^o for K_0=2.0. The comparisons between numerical results and analytical results for coaxial plasticity testify to the correctness of the finite element implementation procedures of the present model. These findings are consistent with conclusions drawn by Yu and Yuan (2006). It is evident that non-coaxial model proposed by Yu and Yuan (2006) is a special case of our model.

Comparison with Discrete Element Modelling simulations

Numerical simulation results by the present model are compared with the results of DEM simulations subject to a simple shear stress path, and results by using the non-coaxial model proposed by Yu and Yuan (2006). The non-coaxial model proposed by

Yu and Yuan (2006), was developed in the content of soil isotropy (the isotropic M-C criterion was adopted) and details can be found in their publication. The DEM tests were carried out by Qian et al (2016) on dense samples using PFC^{2D}. In their DEM simulations, the grains are represented by clumps with a number of 2322, and the inherent anisotropy is produced due to the sample preparation. After isotopically consolidated to 200 kPa, the samples were sheared up to 30% of the shear strain. The local damping coefficient is 0.7. Details of the material properties for the DEM samples can be found in Qian et al (2016).

A constant surface surcharge of p=200 kPa is applied to the finite element modelling by using non-coaxial models. The value of lateral stress ratio ($K_0=\sigma_x/\sigma_y$) is set as $K_0=2.0$ (Handy, 2001). The directions of major principal stress are fixed at different bedding angles at 0°, 15°, 30°, 45°, 60°, 75°, 90° with respect to the x-direction (i.e., 90°- α with respect to the y-direction). The value of the friction angle is obtained by a non-linear regression with DEM data performed in Matlab. The values of Young's Modulus and Poisson's ratio are $E = 2.9 \times 10^4$ kPa and υ=0.15, respectively (Gu, et al., 2017). The coordinate of the anisotropic yield criterion in $(\frac{\sigma_x-\sigma_y}{2}, \sigma_{xy})$ space rotates following the rotating of the bedding angle of the DEM sample. Non-associativity in the conventional flow rule is used with the dilatancy angle $\psi(\Theta_p)=0°$ for simplicity.

Shear stress ratio

Fig. 5 presents results of the stress ratio (shear stress divided by normal stress) plotted against the shear strain in terms of different bedding angles, from both DEM simulations and model predictions. As shown in Fig. 5(a), the evolutions for the stress ratio in terms of different bedding angles are quite similar. They increase rapidly before the shear strain reaches at around 5%, and then decrease with the increase of shearing. All these features of the evolution for the stress ratio are captured by the present model as shown in Fig. 5(b). The peak stress ratios from DEM simulations are within a range of approximately 0.75-0.91, while those from the present model predictions are within a similar range of 0.75-0.89. However, though predictions from Yu and Yuan's non-coaxial model and the M-C model, as shown in Fig. 5(c) and Fig. 5(d) respectively, can capture the softening of the stress ratio, they cannot account for the effect of initial anisotropy (i.e., the bedding angle). The values of the stress ratio are consistent with various bedding angles as shown in Fig. 5(c) and 5(d). The ultimate values for the stress ratio are higher by the model predictions when compared to the DEM simulations. The reason may be that the chosen of non-coaxial coefficient k needs further evaluation, e.g., by HCA testing.

Orientations of principal stresses and principal (plastic) strain rates

DEM simulation results of principal orientations of strain rates are present in Fig. 6(a), of which the polynomial fitting curve is given in Fig. 6(b) as the purple dash line. Seven solid lines corresponding to each bedding angle illustrate the principal orientations of stresses (Fig. 6(b)). As shown in Fig. 6(b), DEM simulation results indicate that non-coaxiality of the principal stress and strain rate exists at the first stage of the loading and tend to be co-axial at around 45°. In addition, different bedding angles (initial anisotropy) result in different directions of principal stresses at the beginning of shearing. However as shown in Fig. 7(a), M-C predictions cannot capture the feature of non-coaxiality, since the directions of principal stress and principal plastic strain rate are always coaxial during shearing. Both predictions from Yu and Yuan (2006) and the present model, demonstrate non-coaxiality of these two directions, as shown in Fig. 7(b) and (c) respectively. Coaxiality of the ultimate orientations of principal stresses and principal (plastic) strain rates are reached and the degrees are around 45°, which are consistent with DEM simulation results and other experimental observations (e.g. Roscoe et al. 1967). However, even for the present model, few differences can be obtained for the directions of principal stresses, with different bedding angles, at the early stage of loading. This discrepancy may result from the fact that only the directions of the principal plastic strain rates are calculated by using the proposed non-coaxial model; however, the total principal strain rate orientations are obtained from the DEM simulations.

CONCLUSIONS

Experimental observations and numerical simulations have shown that non-coaxiality is a significant aspect of soil behaviour, which has not been fully understood. In this paper, a non-coaxial, plane strain soil model has been proposed. The new formulation takes into account the initial soil strength anisotropy. In simple shear tests, perfect agreements with analytical calculations have shown the correctness of the finite element implementation procedures of the newly proposed model. The new model can reproduce the non-coincidence of the direction of the principal stress and principal plastic strain rate when non-associativity in the conventional plastic flow rule was used. This model was capable, however not perfect, of capturing the DEM observations of simple shear testing with respect to the orientations of principal stresses and (plastic) strain rates.

APPENDIX

Conventional part of the plastic strain rate

The conventional part of the plastic strain rate is normal to the plastic potential, and is defined as:

$$\dot{\boldsymbol{\varepsilon}}^{pc} = \dot{\lambda}\ \frac{\partial \mathrm{g}}{\partial \boldsymbol{\sigma}} \tag{15}$$

Where $\dot{\lambda}$ is a positive scalar and g denotes the plastic potential.

Tangential part of the plastic strain rate

The vector $\boldsymbol{T}$ is introduced as normal to the yield surface in the space of ($\frac{\sigma_x-\sigma_y}{2}$, σ_{xy}, $\frac{\sigma_x+\sigma_y}{2}$) , and the material derivative $\dot{\boldsymbol{T}}$ with respect to time depends on the stress rate $\dot{\boldsymbol{\sigma}}$. Following Yu and Yuan (2006) and Harris (1993), the tangential component of the plastic strain rate can be written as follows:

$$\dot{\boldsymbol{\varepsilon}}^{pt} = k \cdot \dot{\boldsymbol{T}} \tag{16}$$

where k is a dimensionless scalar that is introduced as a non-coaxial soil coefficient. The variable m is a geometrical parameter as illustrated in Fig. 2, which can be calculated as follows (Booker and Davis, 1972; Yu, 2007):

$$\tan(2\mathrm{m}) = \frac{1}{2\mathrm{F}}\frac{\partial \mathrm{F}}{\partial \Theta_{\mathrm{p}}} \tag{17}$$

where F is given in Equation 4.

In $(\frac{\sigma_x - \sigma_y}{2}, \sigma_{xy})$ space of an anisotropic yield criterion, the orientation of the normal vector $\boldsymbol{T}$ is introduced as:

$$2\Pi = 2\Theta_p - 2m \tag{18}$$

The material derivative $\dot{\boldsymbol{T}}$ is dependent on both Θ_p and m. Hence, this time T is also influenced by the internal friction angle when compared to the original non-coaxial model proposed by Yu and Yuan (2006).

For a plane strain condition, now the vector $\boldsymbol{T}$ can be written as:

$$\boldsymbol{T} = [cos2\Pi \quad -cos2\Pi \quad 2sin2\Pi]^T \tag{19}$$

The material derivative $\dot{\boldsymbol{T}}$ is then obtained as:

$$\dot{\boldsymbol{T}} = [co\dot{s}2\Pi \quad -co\dot{s}2\Pi \quad 2si\dot{n}2\Pi]^T \tag{20}$$

By combining Equations 16-18 and 20, we can rewrite the material derivative $\dot{\boldsymbol{T}}$ as:

$$\dot{\boldsymbol{T}} = \frac{1}{k} \cdot \boldsymbol{N} \cdot \boldsymbol{\sigma} \tag{21}$$

The matrix $\boldsymbol{N}$ is displayed as follows:

$$\boldsymbol{N} = \begin{bmatrix} a_1 & -a_1 & a_2 \\ -a_1 & a_1 & -a_2 \\ a_3 & -a_3 & a_4 \end{bmatrix} \tag{22}$$

where the scalars a_1, a_2, a_3 and a_4 are presented as:

$$a_1 = k \cdot M \cdot [-\frac{\sigma_{xy}}{4\sigma_{xy}^2 + (\sigma_x - \sigma_y)^2}] \tag{23}$$

$$a_2 = k \cdot M \cdot [\frac{\sigma_x - \sigma_y}{4\sigma_{xy}^2 + (\sigma_x - \sigma_y)^2}] \tag{24}$$

$$a_3 = k \cdot N \cdot [-\frac{\sigma_{xy}}{4\sigma_{xy}^2 + (\sigma_x - \sigma_y)^2}] \tag{25}$$

$$a_4 = k \cdot N \cdot [\frac{\sigma_x - \sigma_y}{4\sigma_{xy}^2 + (\sigma_x - \sigma_y)^2}] \tag{26}$$

where

$$M = -2(\sin 2\Theta_p \cos 2m + \cos 2\Theta_p \sin 2m) \cdot (1 + m_{\Theta_p}) \tag{27}$$

$$N = 2(\cos 2\Theta_p \cos 2m - \sin 2\Theta_p \sin 2m) \cdot (1 + m_{\Theta_p}) \tag{28}$$

With respect to a rotational ellipse in the deviatoric stress space of the anisotropic yield criterion, the definition of $m_{\Theta p}$ is:

$$m_{\Theta_p} = \frac{2(n^2 - 2C + 1) \cdot C - D^2}{C^2} \quad (29)$$

where

$$C = (n^2 - 1)\cos^2(2\Theta_p - 2\beta) + 1 \quad (30)$$

$$D = (1 - n^2)\sin(4\Theta_p - 4\beta) \quad (31)$$

With respect to an eccentric ellipse in the deviatoric stress space of the anisotropic yield criterion, the definition of $m_{\Theta p}$ is:

$$m_{\Theta_p} = \frac{E' \cdot \sqrt{E^2 + F^2} - (\sqrt{E^2 + F^2})' \cdot E}{2\cos(2m) \cdot (E^2 + F^2)}$$

where,

$$E = (n^4 e(1 - n^2)\cos(2\Theta_p) - n^2 e^2)\sin(4\Theta_p) - 2n^2 e S_c S_d \sin(2\Theta_p) - S_c(2 - 2n^2)(S_c + n^2 e\cos(2\Theta_p))\sin(4\Theta_p) \quad (32)$$

$$F = S_c S_d (S_c{}^2 + n^2 e\cos(2\Theta_p)) \quad (33)$$

and,

$$S_c = \sqrt{n^4 (p\sin\phi_{max} + c\cos\phi_{max})^2 \cos^2(2\Theta_p) - n^2 (e^2 - (p\sin\phi_{max} + c\cos\phi_{max})^2)\sin^2(2\Theta_p)} \quad (34)$$

$$S_d = n^2\cos^2(2\Theta_p) + \sin^2(2\Theta_p) \quad (35)$$

$$e = \frac{1}{2}(p + c\cot\phi_{max}) \cdot (\sin\phi_{max} - \sin\phi_p) \quad (36)$$

As a result, the elasto-plastic stress-strain stiffness matrix can be modified to account for both the effects of soil anisotropy and non-coaxiality. The derivatives of stress-strain relationship in the incremental form is shown as follows:

$$\dot{\boldsymbol{\sigma}} = \boldsymbol{D}^{ep}\dot{\boldsymbol{\varepsilon}} = \boldsymbol{D}^{e}(\dot{\boldsymbol{\varepsilon}} - \dot{\boldsymbol{\lambda}}\frac{\partial g}{\partial \boldsymbol{\sigma}} - \boldsymbol{N}\dot{\boldsymbol{\sigma}}) \quad (37)$$

Together with the equation of perfect plasticity under the condition of consistency, the non-coaxial elasto-plastic stress-strain stiffness matrix is shown as:

$$\boldsymbol{D}^{ep} = \frac{\overline{\boldsymbol{D}^e}\frac{\partial g}{\partial \sigma}(\frac{\partial f}{\partial \sigma})^T\overline{\boldsymbol{D}^e}}{(\frac{\partial f}{\partial \sigma})^T\overline{\boldsymbol{D}^e}\frac{\partial g}{\partial \sigma}} \quad (38)$$

where the elastic stiffness matrix $\overline{\boldsymbol{D}^e}$ is modified as:

$$\overline{\boldsymbol{D^e}} = (\boldsymbol{I} + \boldsymbol{D^e N})^{-\mathbf{1}} \boldsymbol{D^e} \tag{39}$$

in which $\boldsymbol{I}$ is introduced as the identity tensor.

ACKNOWLEDGMENTS

This work was supported by the National Natural Science Foundation of China (Grant No. 51609204). The author would like to thank the thesis written by Yuan (2015) for providing the data.

NOTATION

The following symbols are used in this paper:

$\dot{\boldsymbol{\varepsilon}}$	total strain rate
$\dot{\boldsymbol{\varepsilon}}^e$	elastic strain rate
$\dot{\boldsymbol{\varepsilon}}^p$	plastic strain rate
$\dot{\boldsymbol{\sigma}}$	total stress rate
$\boldsymbol{D^e}(\overline{\boldsymbol{D^e}})$	elastic (modified) stiffness matrix
E	Young's modulus
υ	Poisson's ratio
σ_x, σ_y	normal stress
σ_{xy}	shear stress
σ_r	vertical stress
σ_θ	circumferential stress
τ_θ	shear stress in vertical plane
f	yield surface
p	Mean (hydraulic) stress
R,q	deviatoric stress
Θ_p	angle of deviation of the major principal stress direction to the x-axis
ϕ	Internal friction angle
b	intermediate principal stress parameter
$\dot{\lambda}$	positive scalar
g	plastic potential
ψ	dilation angle

c	cohesion
K_0	lateral stress ratio (earth pressure coefficient at rest)
Anisotropic yield criterion	
F	known function of p, Θ_p
Π,m	geometric variables in the anisotropic yield criterion
A/B	The major and minor lengths of the rotational ellipse
$\phi_{max}(\phi_{min})$	maximum (minimum) peak internal friction angle with direction
ϕ_p	Internal friction angle when $\Theta_p = \pi/2$
n	ratio of the minimum over maximum peak internal friction angles
β	angle of the major principal stress direction to the deposition direction
ψ_{max}	maximum dilation angle with direction
Non-coaxial plasticity	
$\dot{\boldsymbol{T}}$	material derivative
N	non-coaxial matrix
$\dot{\boldsymbol{\varepsilon}}^{pc}$	conventional component of the plastic strain rate
$\dot{\boldsymbol{\varepsilon}}^{pt}$	tangential component of the plastic strain rate
k	non-coaxial coefficient

REFERENCES

Abbo, A. J. (1997). "Finite element algorithms for elastoplasticity and consolidation." University of Newcastle Newcastle Upon Tyne.

Ai, J., Langston, P. A., and Yu, H. S. (2014). "Discrete element modelling of material non‐coaxiality in simple shear flows." International journal for numerical and analytical methods in geomechanics, 38(6), 615-635.

Anand, L. (1983). "Plane deformations of ideal granular materials." Journal of the Mechanics and Physics of Solids, 31(2), 105-122.

Arthur, J., Chua, K., and Dunstan, T. (1977). "Induced anisotropy in a sand." Geotechnique, 27(1), 13-30.

Booker, J., and Davis, E. (1972). "A general treatment of plastic anisotropy under conditions of plane strain." Journal of the Mechanics and Physics of Solids, 20(4), 239-250.

Borja, R. I., Sama, K. M., and Sanz, P. F. (2003). "On the numerical integration of three-invariant elastoplastic constitutive models." Computer methods in applied mechanics and engineering, 192(9-10), 1227-1258.

Cai, Y., Yu, H.-S., Wanatowski, D., and Li, X. (2012). "Noncoaxial behavior of sand under various stress paths." Journal of Geotechnical and Geoenvironmental Engineering, 139(8), 1381-1395.

Davis, E. (1968). "Theories of Plasticity and Failure of Soil Masses, Chapter 6, Soil-Mechanics—Selected Topics, Ed. IK Lee." Butterworths.

Drescher, A., and De Jong, G. D. J. (1972). "Photoelastic verification of a mechanical model for the flow of a granular material." Journal of the Mechanics and Physics of Solids, 20(5), 337-340.

Gu, X., Lu, L., and Qian, J. (2017). "Discrete element modeling of the effect of particle size distribution on the small strain stiffness of granular soils." Particuology, 32, 21-29.

Handy, R. L. (2001). "Does lateral stress really influence settlement?" Journal of geotechnical and geoenvironmental engineering, 127(7), 623-626.

Hansen, B. (1961). "Shear box tests on sand." Proc., Proc. 5th Int. Conf. Soil Mechanics Foundation Engineering, Paris, 127-131.

Harris, D. (1993). "Constitutive equations for planar deformations of rigid-plastic materials." Journal of the Mechanics and Physics of Solids, 41(9), 1515-1531.

Hashiguchi, K., and Tsutsumi, S. (2003). "Shear band formation analysis in soils by the subloading surface model with tangential stress rate effect." International Journal of Plasticity, 19(10), 1651-1677.

He, Y., Liu Y., Zhang Y., and Yuan, R. (2019). "Stability assessment of three-dimensional slopes with cracks." Engineering Geology, 252:136-144.

Huang, M., Lu, X., and Qian, J. (2010). "Non-coaxial elasto-plasticity model and bifurcation prediction of shear banding in sands." International journal for numerical and analytical methods in geomechanics, 34(9), 906-919.

Li, X., and Dafalias, Y. (2004). "A constitutive framework for anisotropic sand including non-proportional loading." Geotechnique, 54(1), 41-55.

Neher, H., Cudny, M., Wiltafsky, C., and Schweiger, H. (2002). "Modelling principal stress rotation effects with multilaminate type constitutive models for clay." Numerical Models in Geomechanics, 42.

Pande, G. N., and Sharma, K. (1983). "Multi‐laminate model of clays—a numerical evaluation of the influence of rotation of the principal stress axes." International journal for numerical and analytical methods in geomechanics, 7(4), 397-418.

Qian, J., Yang, J., and Huang, M. (2008). "Three-dimensional noncoaxial plasticity modeling of shear band formation in geomaterials." Journal of engineering mechanics, 134(4), 322-329.

Qian, J., Li, W., Gu, X., and Xu, K. (2016). "Influence of Inherent Anisotropy on the Soil Behavior in Simple Shear Tests Using DEM." Proc., International Conference on Discrete Element Methods, Springer, 777-784.

Roscoe, K. H. (1970). "The influence of strains in soil mechanics." Geotechnique, 20(2), 129-170.

Roscoe, K. H., Bassett, R.H., Cole, E.R.L. (1967). "Principal axes observed during simple shear of a sand." Proc. Geotech. Conf. Oslo, 1, 231-237.

Rudnicki, J. W., and Rice, J. (1975). "Conditions for the localization of deformation in pressure-sensitive dilatant materials." Journal of the Mechanics and Physics of Solids, 23(6), 371-394.

Sadrnejad, S., and Shakeri, S. (2017). "Multi-laminate non-coaxial modelling of anisotropic sand behavior through damage formulation." Computers and Geotechnics, 88, 18-31.

Savage, J., and Lockner, D. (1997). "A test of the double‐shearing model of flow for granular materials." Journal of Geophysical Research: Solid Earth, 102(B6), 12287-12294.

Spencer, A. (1964). "A theory of the kinematics of ideal soils under plane strain conditions." Journal of the Mechanics and Physics of Solids, 12(5), 337-351.

Tejchman, J., and Wu, W. (2009). "Non‐coaxiality and stress‐dilatancy rule in granular materials: FE investigation within micro‐polar hypoplasticity." International journal for numerical and analytical methods in geomechanics, 33(1), 117-142.
Tong, Z.-X., Zhang, J.-M., Yu, Y.-L., and Zhang, G. (2010). "Drained deformation behavior of anisotropic sands during cyclic rotation of principal stress axes." Journal of Geotechnical and Geoenvironmental Engineering, 136(11), 1509-1518.
Tsutsumi, S., and Hashiguchi, K. (2005). "General non-proportional loading behavior of soils." International Journal of Plasticity, 21(10), 1941-1969.
Wu, Y., Zhou, X., Gao Y., Zhang, L., and Yang, J. (2019). "Effect of soil variability on bearing capacity accounting for non-stationary characteristics of undrained shear strength." Computer and Geotechnics, 110:199-210.
Yang, L. (2013). "Experimental study of soil anisotropy using hollow cylinder testing." University of Nottingham.
Yang, Y., and Yu, H. (2006a). "Numerical simulations of simple shear with non-coaxial soil models." International journal for numerical and analytical methods in geomechanics, 30(1), 1-19.
Yang, Y., and Yu, H. (2006b). "A non-coaxial critical state soil model and its application to simple shear simulations." International journal for numerical and analytical methods in geomechanics, 30(13), 1369-1390.
Yang, Y., and Yu, H. (2006c). "Application of a non-coaxial soil model in shallow foundations." Geomechanics and Geoengineering: An International Journal, 1(2), 139-150.
Yang, Y., and Yu, H.-S. (2010). "Numerical aspects of non-coaxial model implementations." Computers and Geotechnics, 37(1-2), 93-102.
Yu, H.-S. (2007). Plasticity and geotechnics, Springer Science & Business Media.
Yu, H., and Yuan, X. (2006). "On a class of non-coaxial plasticity models for granular soils." Proc., Proceedings of the Royal Society of London A: Mathematical, Physical and Engineering Sciences, The Royal Society, 725-748.
Yuan, R., Yu, H.-S., Hu, N., and He, Y. (2018). "Non-coaxial soil model with an anisotropic yield criterion and its application to the analysis of strip footing problems." Computers and Geotechnics, 99, 80-92.
Zhang, L. (2003). "The behaviour of granular material in pure shear, direct shear and simple shear." Aston University.

Fig. 1 The anisotropic yield surface in: (a) X=(σ_x-σ_y)/2, Y=σ_{xy}, Z=(σ_x+σ_y)/2 space; (b) X=(σ_x-σ_y)/2, Y=σ_{xy} space.

Fig. 2 The yield surface and non-coaxial plastic flow rule in: (a) ((σ_x-σ_y)/2, σ_{xy}, (σ_x+σ_y)/2) space, (b) ((σ_x-σ_y)/2, σ_{xy}) space.

Fig. 3 Numerical results of shear stress ratio for isotropic modelling (n=1): (a) associativity; (b) non-associativity.

Fig. 4 Numerical results of principal orientations of the stress and plastic strain rate for coaxial modelling (n=1, k=0): (a) associativity, (b) non-associativity.

Fig.5 Shear stress ratio against the shear strain: (a) DEM simulation results (Qian et al., 2016); (b) numerical results by the present model; (c) numerical results by the non-coaxial (Yu and Yuan, 2006); (d) numerical results by the Mohr-Coulomb model.

Fig.6 DEM simulation results (Qian et al., 2016): (a) principal orientations of strain rates; (b) principal stress orientations and the fitted principal strain orientation.

Fig.7 Model predictions for the principal orientations of stresses and plastic strain rates: (a) Mohr-Coulomb model; (b) non-coaxial model (Yu and Yuan, 2006); (c) the present model.

Table 1 Model parameters.

Young's modulus	Poisson's ratio	maximum internal friction angle	Surface surcharge	Lateral stress ratio	
E (kPa)	υ	$\phi_{\max}$ (°)	p (kPa)	K_0	
2.6×10^4	0.3	30	100	0.5	2.0

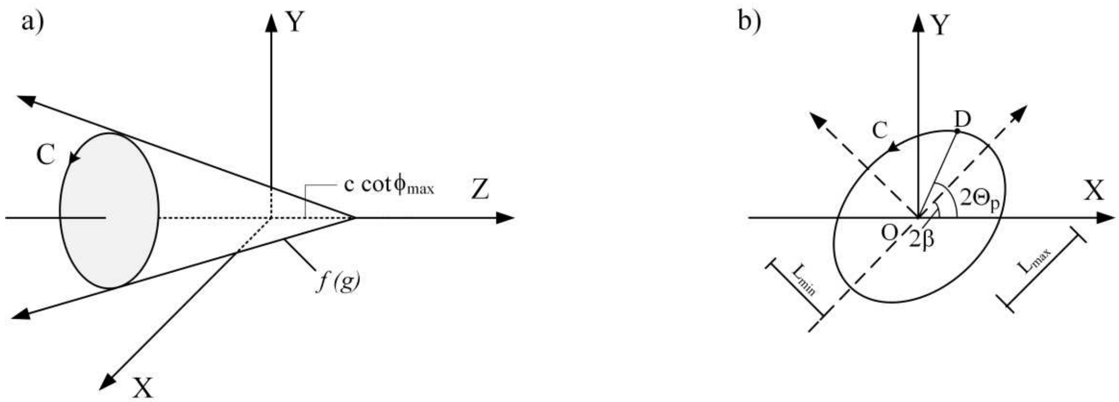
a)
Y
C
c cotϕ_{max}
Z
$f(g)$
X
b)
Y
D
C
X
$2\Theta_p$
O
2β
L_{min}
L_{max}

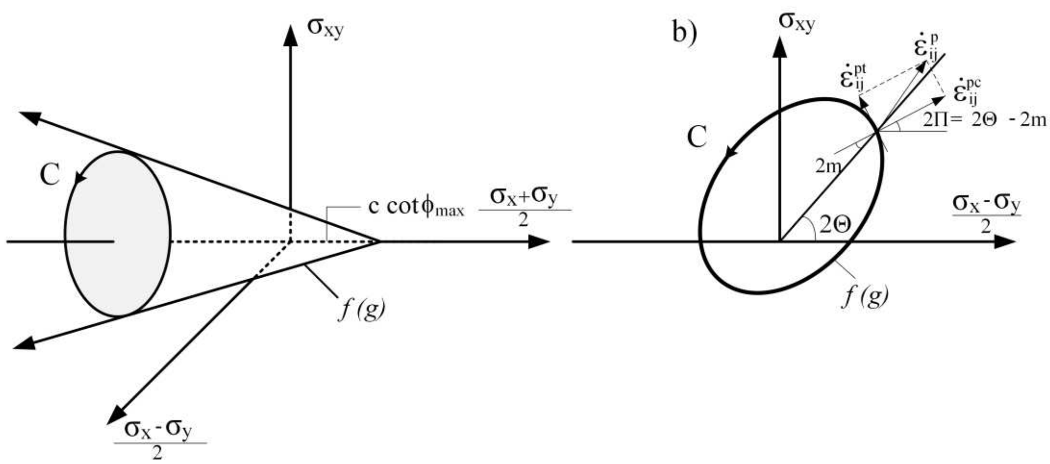
a)
σ_{xy}
C
c cotϕ_{max}
$\frac{\sigma_x+\sigma_y}{2}$
$f(g)$
$\frac{\sigma_x-\sigma_y}{2}$
b)
σ_{xy}
$\dot{\varepsilon}_{ij}^{p}$
$\dot{\varepsilon}_{ij}^{pt}$
$\dot{\varepsilon}_{ij}^{pc}$
$2\Pi = 2\Theta - 2m$
C
2m
2Θ
$\frac{\sigma_x-\sigma_y}{2}$
$f(g)$

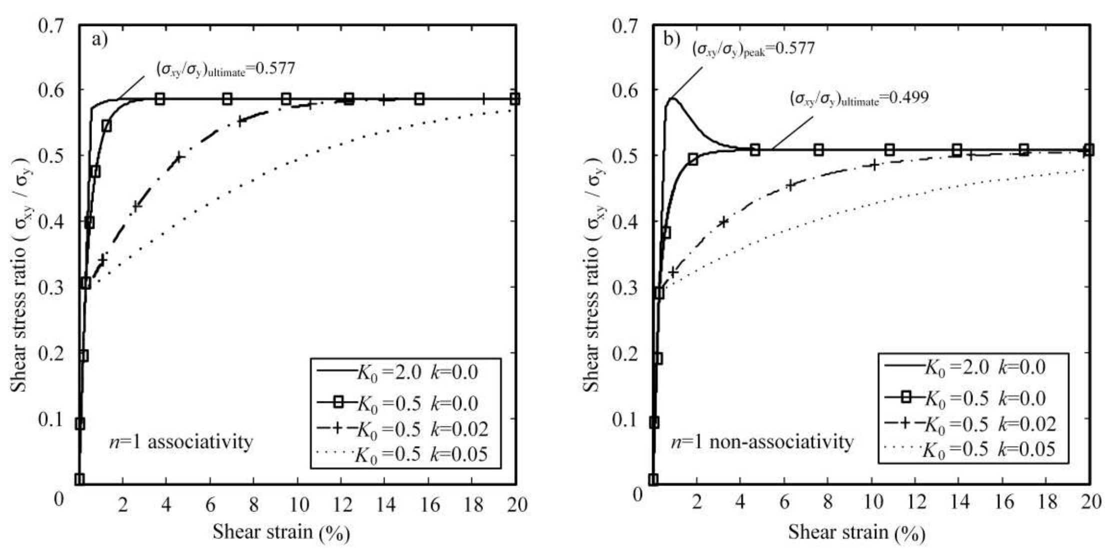
a)
$(\sigma_{xy}/\sigma_y)_{ultimate}$=0.577
Shear stress ratio (σ_{xy} / σ_y)
Shear strain (%)
K_0=2.0 k=0.0
K_0=0.5 k=0.0
K_0=0.5 k=0.02
K_0=0.5 k=0.05
n=1 associativity
b)
$(\sigma_{xy}/\sigma_y)_{peak}$=0.577
$(\sigma_{xy}/\sigma_y)_{ultimate}$=0.499
Shear stress ratio (σ_{xy} / σ_y)
Shear strain (%)
K_0=2.0 k=0.0
K_0=0.5 k=0.0
K_0=0.5 k=0.02
K_0=0.5 k=0.05
n=1 non-associativity

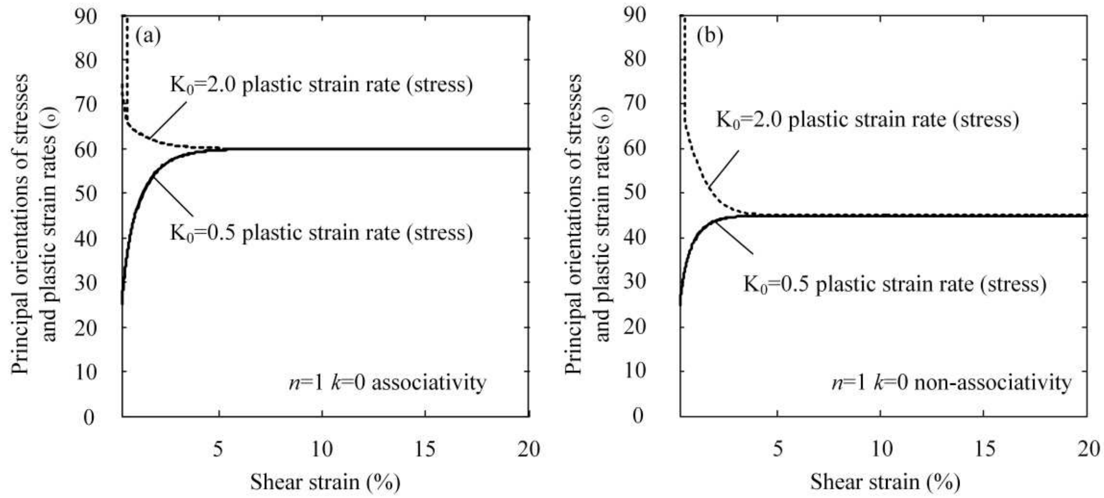

(a)
(b)
Principal orientations of stresses and plastic strain rates (o)
K0=2.0 plastic strain rate (stress)
K0=0.5 plastic strain rate (stress)
n=1 k=0 associativity
n=1 k=0 non-associativity
Shear strain (%)

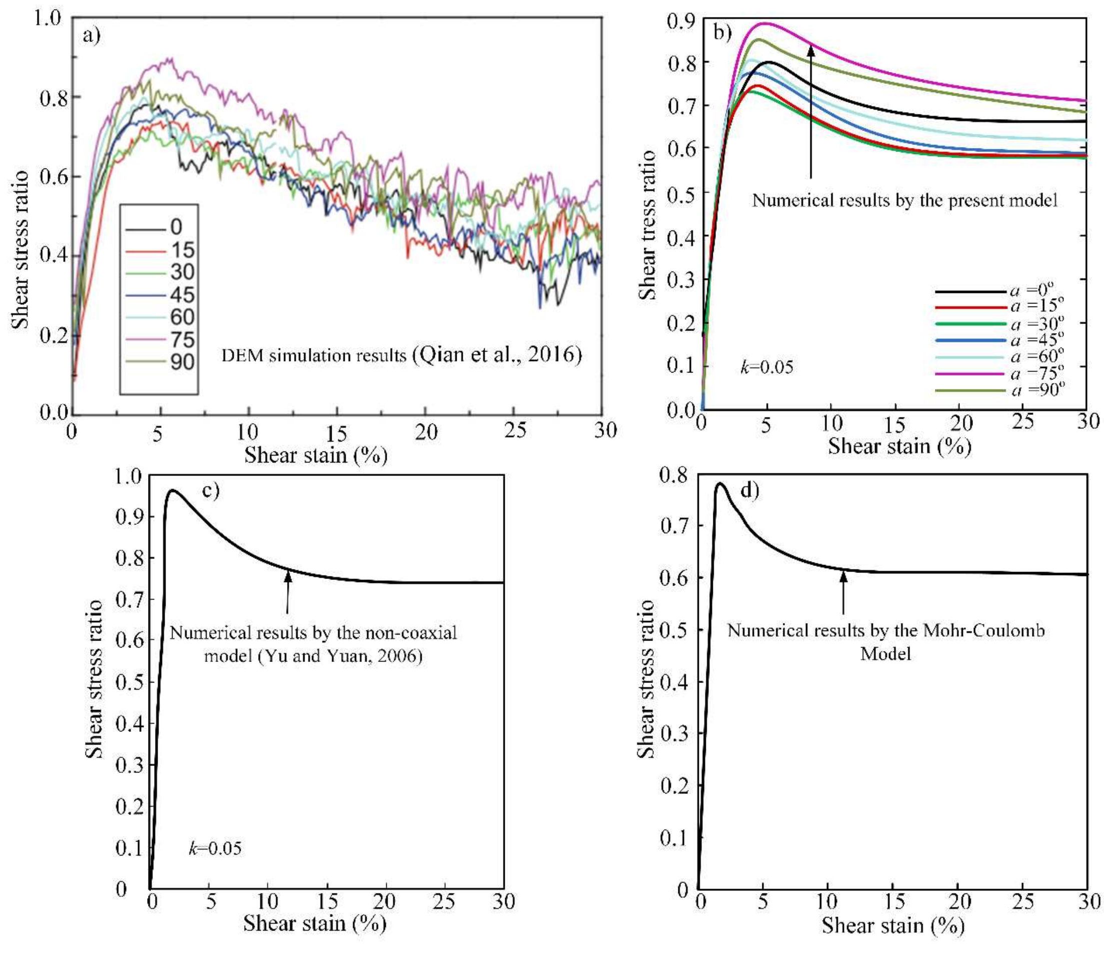

a)
b)
c)
d)
Shear stress ratio
Shear tress ratio
0
15
30
45
60
75
90
DEM simulation results (Qian et al., 2016)
Numerical results by the present model
a =0°
a =15°
a =30°
a =45°
a =60°
a =75°
a =90°
k=0.05
Numerical results by the non-coaxial model (Yu and Yuan, 2006)
Numerical results by the Mohr-Coulomb Model
Shear stain (%)

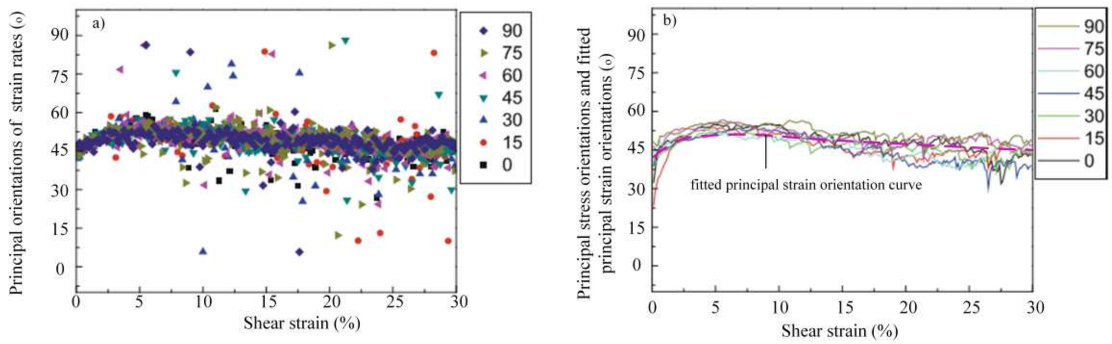

a)
Principal orientations of strain rates (o)
Shear strain (%)
90
75
60
45
30
15
0
b)
Principal stress orientations and fitted principal strain orientations (o)
fitted principal strain orientation curve
Shear strain (%)

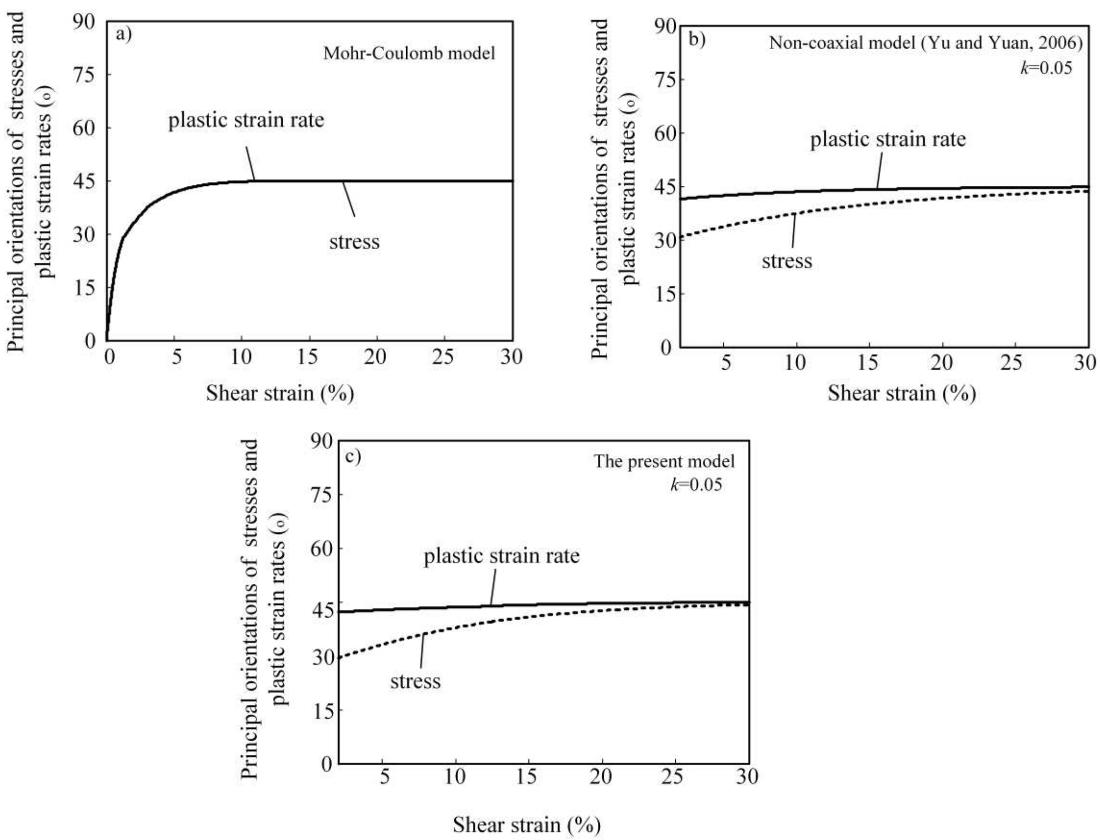

a)
Mohr-Coulomb model
plastic strain rate
stress
Principal orientations of stresses and plastic strain rates (o)
Shear strain (%)
b)
Non-coaxial model (Yu and Yuan, 2006)
k=0.05
plastic strain rate
stress
Principal orientations of stresses and plastic strain rates (o)
Shear strain (%)
c)
The present model
k=0.05
plastic strain rate
stress
Principal orientations of stresses and plastic strain rates (o)
Shear strain (%)